Building Tomorrow's Society
Bâtir la Société de Demain

Fredericton, Canada
June 13 – June 16, 2018/ *Juin 13 – Juin 16, 2018*

SEISMIC PERFORMANCE OF SHEAR CONTROLLED SRC COMPOSITE COLUMNS IN EXISTING BUILDINGS

M. Farag[1], W.Hassan[2,3]
[1] Research Assistant, American University in Cairo, Egypt, mayer@aucegypt.edu
[2] Adjunct Assistant Professor, Housing & Building National Research Center, Cairo, Egypt
[3] waelhassan@aucegypt.edu

Abstract: This paper address experimentally the cyclic performance of older-type steel reinforced concrete (SRC) columns that resemble existing buildings and bridges of pre 1980s construction; prior to enforcing seismic details. Two tests specimens representing exterior columns modeled based on a typical seismic design of a 20-story prototype gravity-designed existing building are constructed and tested under quasi-static cyclic loading with different axial compression loads. The tested columns include non-seismic widely spaced hoops with 90 degree hooks; thus the columns are considered flexure and confinement deficient. Test parameters include target failure mode and axial load ratio. The tests aim to quantify existing SRC columns seismic strength and deformability along with a preliminary attempt to establish backbone curve recommendations. From performance-based engineering demand viewpoint, the results show very satisfactory drift capacity associated with low axial load ratio and limited drift capacity and progressive strength and stiffness degradation under high axial load ratio.

Keywords: SRC columns; flexural failure; seismic assessment; existing buildings; non-ductile concrete.

1.0 Introduction

The existing building stock in many active seismic regions includes many seismically deficient buildings that were constructed without enforcing seismic details in the 1980s. Many existing buildings and bridges utilize SRC columns, with structural steel sections embedded in concrete that are not seismically detailed. Literature reveals a serious lack of knowledge on the behavior of SRC composite columns subjected to simulated seismic loading conditions. There are a small number of tests available to justify deriving seismic backbone curves for macro modeling or retrofitting purposes. Numerical criteria to distinguish the seismic modes of failure of such columns are also absent. In addition, no information on the residual axial capacity of SRC composite columns following shear or flexural failure can be drawn from the few tests available in the literature due to premature test termination.

Ricleet al. (1992) tested six SRC column specimens to quantify lateral stiffness, transverse shear resistance, level of concrete confinement, and the effectiveness of shear studs in resisting lateral loading. Chen et al. (2007) conducted an experimental study on twenty six specimens to study the seismic behavior of SRC composite members and their influence parameters. They used three steel section shapes and changed the parameters of axial load ratio, longitudinal steel ratio, steel section ratio, embedded steel section length, and transverse steel ratio. It is noteworthy that most of the tested specimens in these two studies resembled modern construction practices not the older ones. According to the results of these two studies, longitudinal bar buckling must be prevented to preserve the integrity of the member, the axial compression ratio is an important factor that affects the seismic behavior of steel concrete columns, hoop ratio is very significant in the seismic behavior of SRC columns, and the minimum value of the embedded depth of steel concrete composite column can be 2.5 times the section depth. No recommendations for the

backbone curves or performance acceptance criteria were made in these studies. In the current paper, an experimental program consisting of two large-scale test specimens is conducted to address the seismic strength and deformation capacities along with residual axial capacity of flexural controlled SRC columns lacking seismic details.

2.0. Test Matrix and Material Properties

A 20 story prototype building mimicking gravity designed older construction was used to obtain the seismic demands on an existing flexural controlled exterior column. According to ACI 318-63, the composite column design equation does not differ from the current ACI 318-14 equation. However, the main difference is the steel section ratio, which is 5%-9% Ac (where Ac is gross concrete area) in older code versus 1%-3%Ac in ACI 31814 code, and the longitudinal steel ratio, which is 2%-3%Ac in the older code instead of 1%-2%Ac in the modern one. Locally produced ready mixed concrete of 27 MPa characteristic strength was used to construct the test specimens. Actual yield strength of longitudinal steel bars and transverse hoops were 428 MPa and 516 MPa, respectively, while that of the steel section was 435 MPa.

The current tests aimed to study the cyclic performance of flexural and shear controlled SRC columns and establish the flexure and shear deformation capacities and backbone curves for such columns. Four large-scale SRC columns were constructed with the concrete dimensions and steel details depicted in Fig.1.Specimen transverse reinforcement comprised 90 degree hook hoops spaced at 75 mm. The specimen matrix and material properties are shown in Table 1. The specimens were tested in single curvature bending with two axial load ratios (ALR) of 15% and 80%. The ALR is the ratio between axial load and the gross concrete section capacity based on cylinder compressive strength.

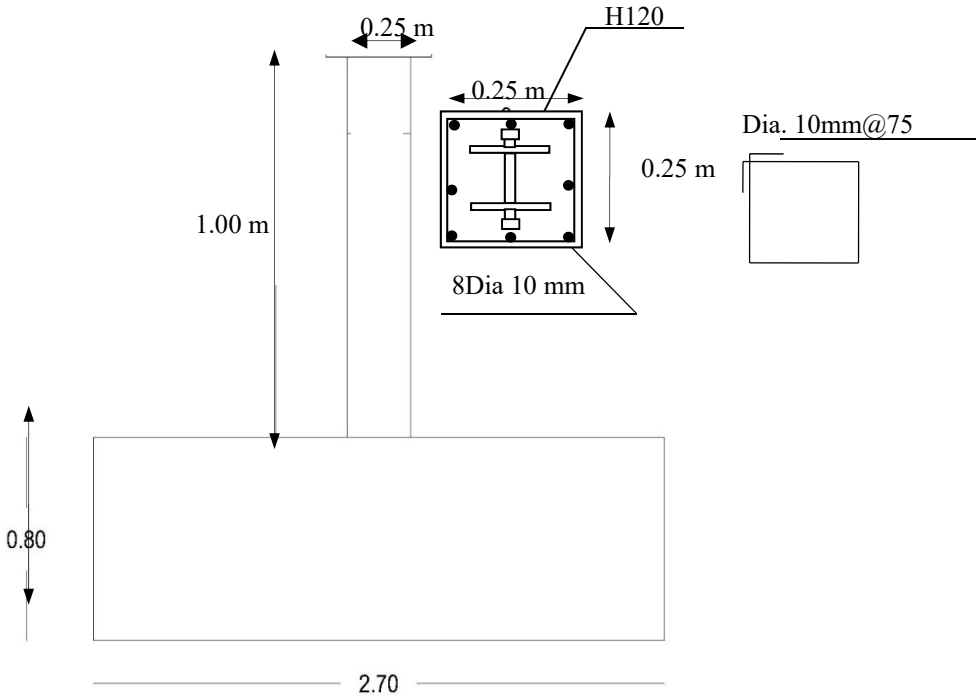

Figure 1: Test specimen details (flexure deficient)

0.25m

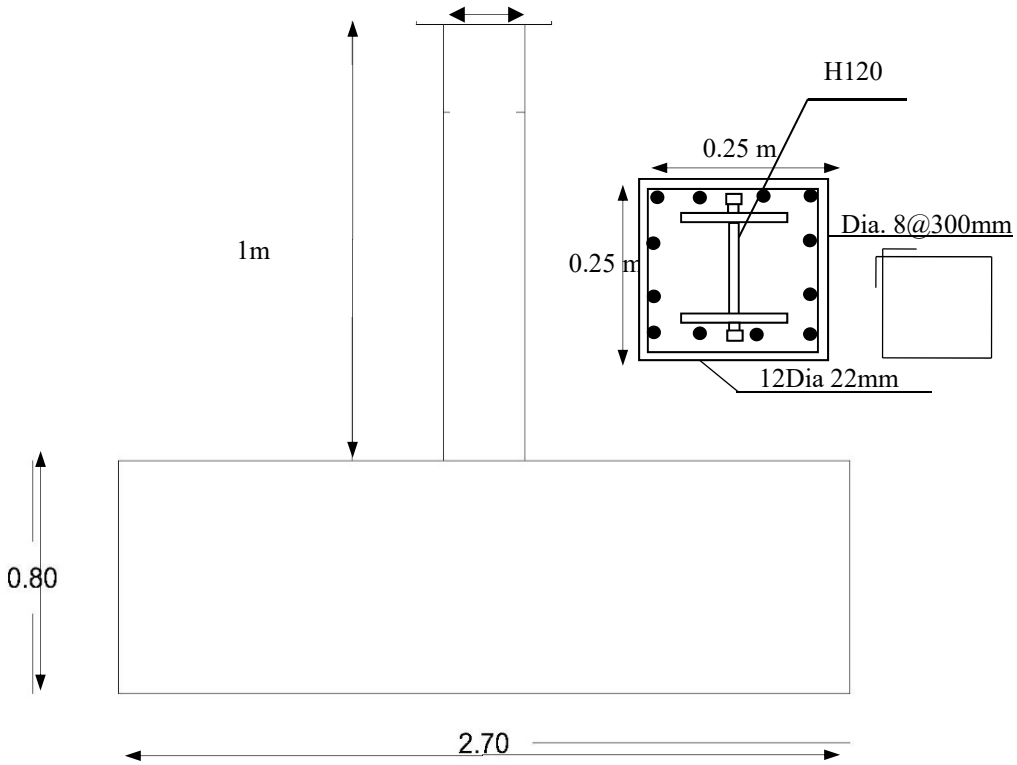

Figure 2: Test specimen details (shear deficient)

Table 1: Flexure deficient specimens test matrix

Specimen ID	*fc'* MPa	Target Failure Mode	ALR	Hoop Spacing	Steel Section Ratio	Reinforcement Steel Ratio
F15	27.9	Flexure	0.15	S=7.5 cm	5.44% (H120)	1% (8Φ10)
F80	27.6	Flexure	0.80	S=7.5 cm	5.44% (H120)	1% (8Φ10)

Table 2: Shear deficient specimens test matrix

Specimen ID	*fc'* MPa	Target Failure Mode	ALR	Hoop Spacing	Steel Section Ratio	Reinforcement Steel Ratio
S40	26.7	Shear	0.40	S=30 cm	5.44% (H120)	7.33% (12Φ22)
S80	27.2	Shear	0.80	S=30 cm	5.44% (H120)	1% (12Φ22)

3. Test Setup and Loading Protocol

The test setup comprises a horizontal 220 kN dynamic actuator with a 120 mm tension and compression stroke capacities supported to a strong wall and applying lateral load at the top of the specimen as shown in Fig. 2. The lateral loading rate was 0.5 mm per second. A 2000 kN vertical load cell connected to a vertical jack that is attached to a loading frame and braced laterally to the reaction wall was used to apply the axial load. A rolling mechanism was introduced to allow for sliding of the column top under the vertical load. The test setup is shown in Fig. 3. The test was performed under quasi-static displacement controlled protocol until lateral failure followed by axial failure is reached. The displacement protocol was derived based on multiples of the theoretical yield displacement and is shown in Fig. 4.Two displacement cycles were used prior to reaching theoretical yield displacement followed by three cycles per each displacement amplitude after reaching the theoretical yield displacement. The yield displacement for flexural controlled specimens is calculated by summation of slip, plastic and elastic displacements at section yield predicted using memento-curvature analysis. Seven strain gages and seven LVDTs were used to instrument each test specimen at critical strain locations. A data controller and acquisition systems were used to apply and monitor loading conditions and collect the test data results.

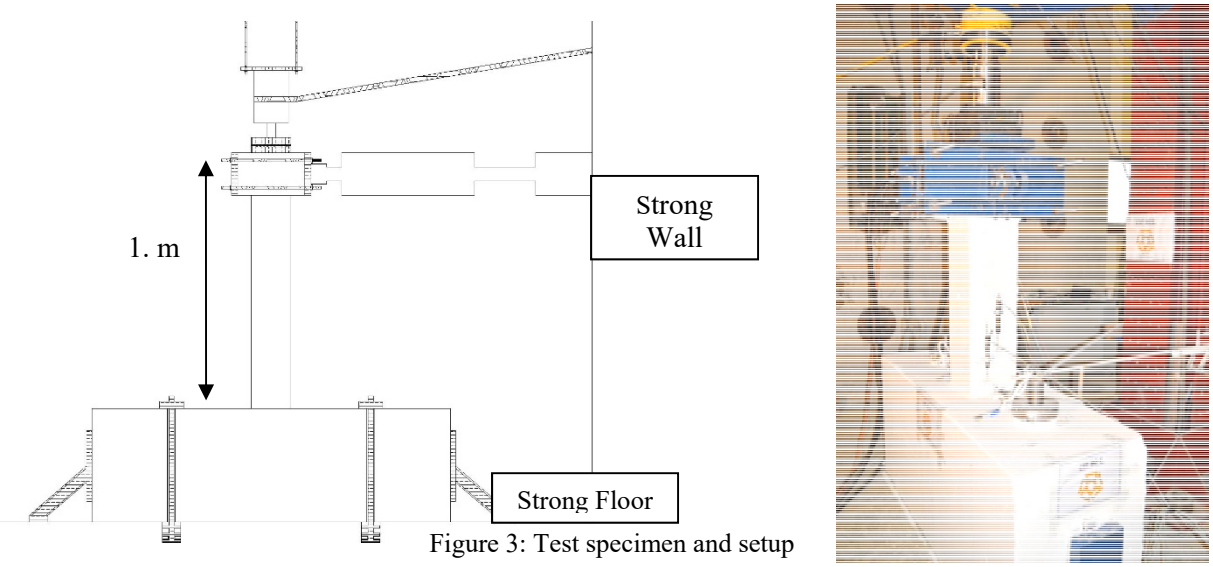

Figure 3: Test specimen and setup

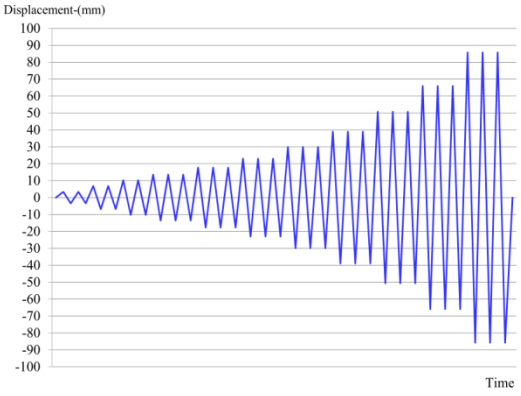

Figure 4: Displacement protocol

4. Experimental Results

Figure 5 shows the failure mode of specimen F15 under the effect of the applied displacement protocol and a constant axial load ratio of 15%. Flexure cracks appeared as early as 0.7% drift ratio. Flexure cracks then progressed on two opposite sides of the specimens especially cracks located in the area of d/2 from base of column. The major cracks width kept increasing while the specimen started to lose its lateral load capacity. One longitudinal bar in each direction of loading ruptured. The test was continued until axial failure was reached which was identified by severe concrete spalling, buckling of longitudinal bars, opening of hoops and significant sudden loss of vertical axial load (more than 30% loss) .

Figure 5: Failure mode of specimen F15

Figure 6 shows the shear force-drift ratio hysteresis response of specimen F15. The peak shear capacity of the specimen was 161kN. This exceeded the theoretically predicted flexural capacity of 111 kN. The peak shear capacity was reached at 4.6% drift ratio. The test was continued until 6.1% drift ratio, at which axial failure was identified. This drift ratio is considered relatively high for the typical reinforced concrete existing buildings (with no conventional concrete columns) which generally can tolerate less than 2% drift before collapse. The 4.6% peak lateral load drift capacity is considered satisfactory if judged by TBI acceptance criteria for modern columns under Maximum Considered Earthquake (MCE) single record which is 4.5% and significantly acceptable if compared to the mean MCE acceptance criteria for several records which is 3%.The axial failure was reached at 6.1% drift ratio when the axial stability was lost due to cutting of two steel bars and buckling of other longitudinal bars. Thus, drift capacity corresponding to axial load ratio of 15% was 6.1% inter story drift ratio.

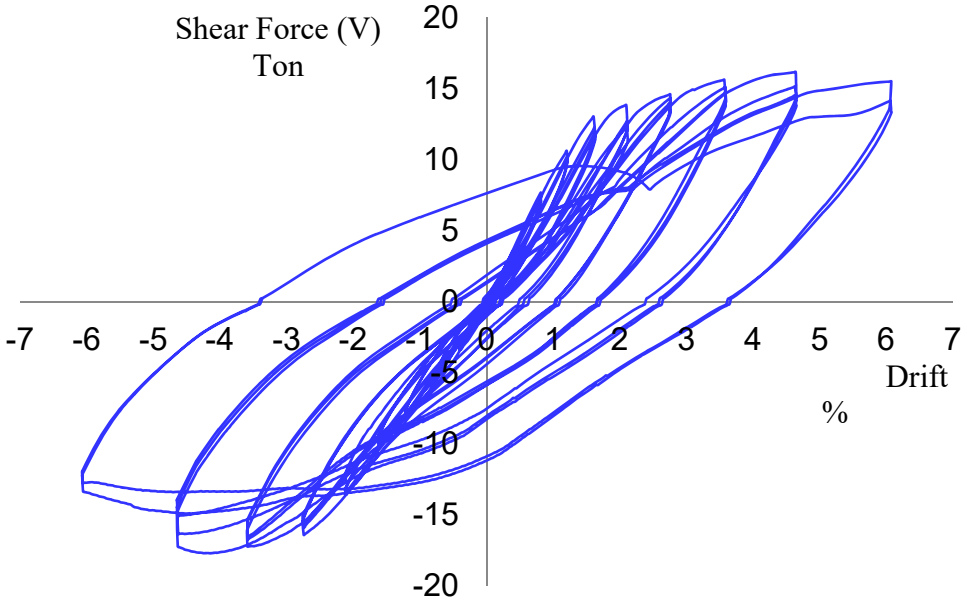

Figure 6: Shear force-drift hysteresis response of specimen F15

Figure 7 shows the failure mode of specimen F80 under the effect of the applied displacement protocol associated with constant axial load ratio of 80%. The failure mode of specimen was a confirmed flexure failure characterized by significant flexure cracking on two sides of the specimen with an aggressive flexure cracks that kept widening with the displacement protocol in the area of d/2 from the column base. The failure mode of this specimen was similar to that of specimen F15 except that there were not any bars failed during the test but it was like a surprise to find that flanges of steel section buckled with the same deformation shape of longitudinal bars deformation and also the opening of transverse hoops lead to to crush in the concrete in compression.

Figure 7: Failure mode of specimen F80

Figure 8 shows the shear force-drift ratio hysteresis response of specimen F80. The peak shear strength reached was 178 kN which is significantly higher than the 128 kN theoretically predicted shear strength of AISC 314. Obviously, the increase in the axial load ratio from 15% in specimen F15 to 80% in specimen F8 results an increase in peak shear strength. However, the loading stiffness of specimen F80 is obviously higher than that of specimen F15 as can be clearly observed from Fig. 9, which shows the backbone curves of the two specimens in the positive (initial) loading direction. This is attributed to the higher axial load ratio effect in increasing axial stiffness. The peak shear strength was reached at 2% drift ratio, which is about 57% less than that of specimen F15, emphasizing the effect of higher axial load in limiting the deformability and energy dissipation of the test specimen. This can be also observed by comparing the fatness of the hysteresis loops in specimen F15 compared to those in specimen F80. Moreover, the axial failure drift capacity of specimen F80 was 4.5% which is about 26% less than the 6.1% drift capacity of specimen F15. This further indicates the limited seismic deformation capacity imposed by the higher axial load in F80 specimen. The post peak shear strength degradation in specimen F80 is higher than that of specimen F15 confirming the same observation.

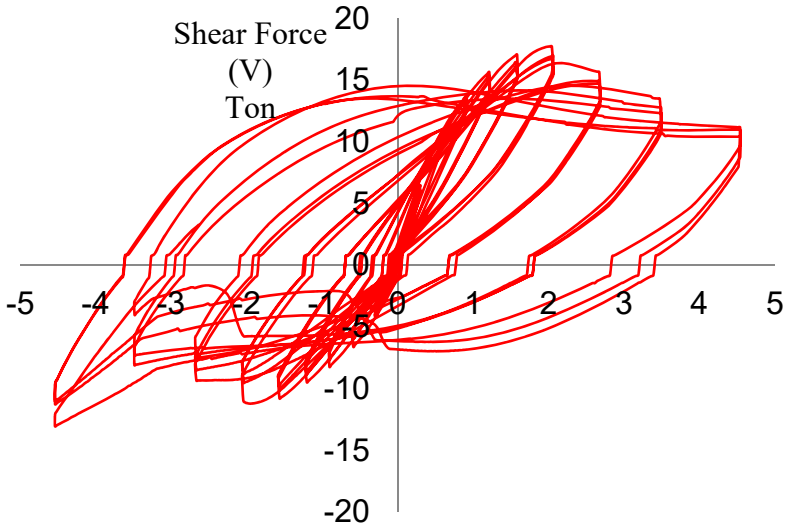

Figure 8: Shear force-drift ratio hysteresis response of specimen F80

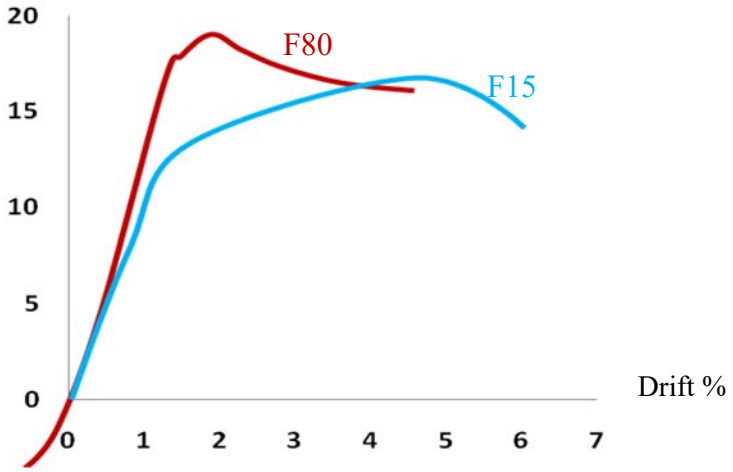

Figure 9: Envelop curves of test specimens

Figure 10 shows the failure mode of specimen S40 under the effect of the applied displacement protocol and a constant axial load ratio of 40%. Shear cracks appeared as early as 1.7% drift ratio. Shear cracks then progressed on two opposite sides of the specimens with two main cracks and several minor cracks. The main crack width kept increasing while the specimen started to lose its lateral load capacity. The test was continued until axial failure was reached, which was identified by substantial concrete spalling, buckling of longitudinal bars, opening of transverse hoops and significant loss of vertical axial load.

Figure 10: Failure mode of specimen S40

Figure 11 shows the shear force-drift ratio hysteresis response of specimen S40. The peak shear capacity of the specimen was 225 kN. This significantly exceeded the theoretical shear prediction value of AISC 341 which was 137 kN (based on concrete and hoop shear resistance). It is noteworthy that code shear capacity is believed to be based on first shear cracking capacity. The peak shear capacity was reached at 2.88% drift ratio. It is usually accepted to consider the shear failure has occurred when 80% of lateral load capacity is reached. Thus, the 20% loss in lateral force capacity was reached at 4.2% drift ratio. This drift ratio is considered relatively high for the typical reinforced concrete existing buildings (with conventional RC columns) which generally can tolerate less than 2% drift before collapse. However, this peak drift ratio is considered low if compared to the new building collapse prevention drift limit state of 4.5% for a single ground motion and 3% for the mean of several ground motions, as per recommended by Tall Building Initiative (2011). The specimen exhibited brittle shear failure with immediate strength degradation following the peak shear strength. The axial failure was reached at 5% drift ratio when the axial stability was lost due to opening of transverse hoops and buckling of longitudinal bars and severe uneven loss of concrete which led to axial load eccentricity and significant drop in axial capacity (more than 25%) associated with out of plane twisting of the specimen. Thus, drift capacity corresponding to axial load ratio of 40% was 5% inter story drift ratio.

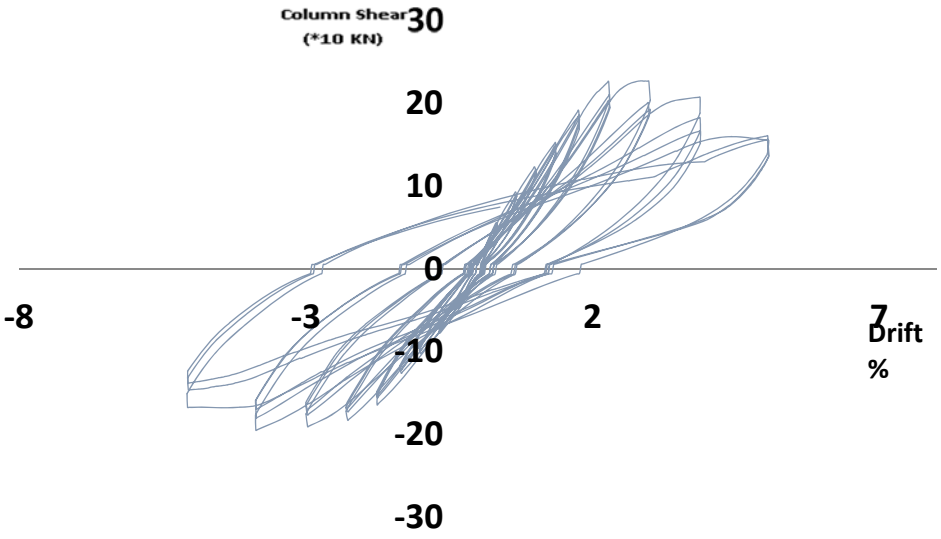

Figure 11: Shear force-drift hysteresis response of specimen S40

Figure 12 shows the failure mode of specimen S80 under the effect of the applied displacement protocol associated with constant axial load ratio of 80%. The failure mode of specimen was a confirmed shear failure characterized by significant shear cracking on two sides of the specimen with two major shear cracks that kept widening with the displacement protocol progression along with a few minor shear cracks. The failure mode of this specimen was an exaggerated version of that of specimen S40 except that several vertical cracks appeared towards the end of the test signifying cover splitting forces resulting from substantial axial load ratio. The vertical cracks then joined the shear cracks and were associated with concrete chunks spalling and buckling of longitudinal bars associated with significant drop in the axial load carrying capacity to bring the specimen to axial failure.

Figure 12: Initial and final failure mode of specimen S80

Figure 13 shows the shear force-drift ratio hysteresis response of specimen S80. The peak shear strength reached was 215 kN which is significantly higher than the 158 kN theoretically predicted shear strength of AISC 341. Counter intuitively, the increase in the axial load ratio from 40% in specimen S40 to 80% in specimen S80 did not result in an increase in peak shear strength. However, the loading stiffness of specimen S80 is obviously higher than that of specimen S40 as can be clearly observed from Fig. 14, which shows the backbone curves of the two specimens in the positive (initial) loading direction. This is attributed to the higher axial load ratio effect in increasing axial stiffness. The peak shear strength was reached at 2.28% drift ratio, which is about 21% less than that of specimen S40, emphasizing the effect of higher axial load in limiting the deformability and energy dissipation of the test specimen. This can be also observed by comparing the fatness of the hysteresis loops in specimen S40 compared to those in specimen S80. Moreover, the axial failure drift capacity of specimen S80 was 3.86% which is about 24% less than the 5% drift capacity of specimen S40. This further indicates the limited seismic deformation capacity imposed by the higher axial load in S80 specimen. The post peak shear strength degradation in specimen S80 is higher than that of specimen S40 confirming the same observation. The axial failure corresponded to a 30% drop in the lateral load capacity in specimen S40 while it corresponded to 25% drop in lateral load

capacity in specimen S80. The drift ratio corresponding to reaching 20% shear strength degradation in specimen S80 was 3.5%, which is 23% less than its counterpart in specimen S40. This 3.5% reduced drift capacity is deemed relatively high compared to its counterpart in existing reinforced concrete buildings undergoing strong shaking and experiencing column shear failure, however, it is considered insufficient if compared to the modern building seismic drift capacity requirements under collapse prevention limit state as recommended by Tall Building Initiative (2011). Thus, retrofitting such shear deficient columns experiencing moderate to strong ground shaking under high axial loads seems inevitable.

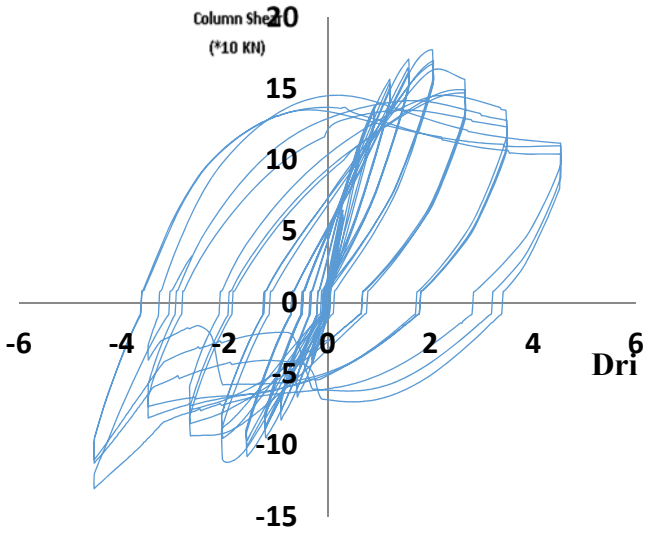

Figure 13: Shear force-drift ratio hysteresis response of specimen S80

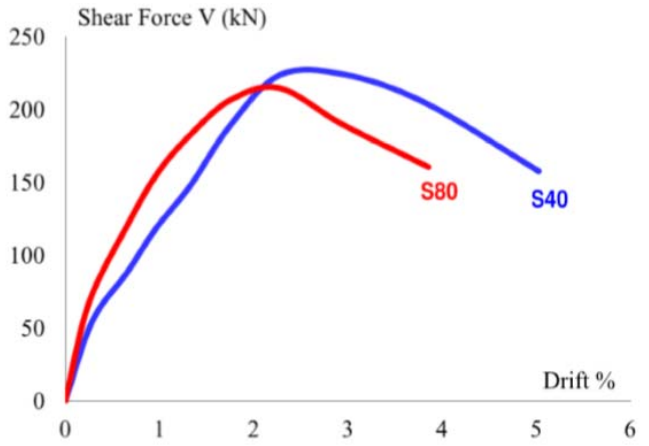

Figure 14: Envelop curves of test specimens

4.0. Conclusion

Based on the observation of failure modes and test results, the following conclusions could be drawn:
Shear Conclusion:

1. The steel section web and shear studs works to over-strength the column in shear.
2. Although, the specimens represented the existing building, showed a very satisfied shear capacity, the failure drift is not safe according to ACI 1963. So, there are many existing composite building are not safe.
3. Flexural tension test for specimen F15 shows that loading with low axial load ration led to total failure of some steel bars.
4. The test shear strength of both specimens significantly exceeded the theoretical prediction of AISC 341 by about 45%-49%.
5. The low axial load ration let the specimen reach to a high peak drift ratio reached to 4.6% and this is a very satisfied ratio for an existing building without any seismic details
6. Increasing the axial load ratio from 15% to 80% shows a very different behaviour of failure as the high axial load ratio led to the deformation flanges and opening the hoops transverse..
7. Increasing the axial load ratio from 15% to 80% was detrimental to deformation capacity of test specimens. It reduced peak shear drift by 57%, axial failure drift by 27% and resulted in faster post peak shear strength degradation.

Flexure conclusion:

1. The hoop deficient SRC columns experienced early shear failure under cyclic load reversals and high axial load ratios.
2. The test shear strength of both specimens significantly exceeded the theoretical prediction of AISC 341 by about 36%-64%.
3. The tested specimens exhibited early shear failure at relatively low drift ratios of 2.28%-2.88%, which implies that SRC existing buildings are not fully compliant with modern building collapse prevention drift requirements under strong shaking. Thus, retrofitting such columns is strongly suggested.
4. Increasing the axial load ratio from 40% to 80% did not help gain higher shear strength as intuitively predicted and codified by AISC 341.
5. Increasing the axial load ratio from 40% to 80% was detrimental to deformation capacity of test specimens. It reduced peak shear drift by 21%, axial failure drift by 24% and resulted in faster post peak shear strength degradation

References

ACI 318-63. Building Code Requirements for Structural Concrete, American Concrete Institute, MI, USA.
ACI 318-14. Building Code Requirements for Structural Concrete, American Concrete Institute, MI, USA.
AISC 341-08. Specification for Seismic Design of Structural Steel, American Institute for Steel Construction, USA.
Chen, C., Wang, C., Sun, H., 2014. Experimental Study on Seismic Behavior of Full Encased Steel-Concrete Composite Columns, ASCE Journal of Structural Engineering, Vol. 140.
Farag, M., and Hassan, W. 2015. Seismic Performance of Steel Reinforced Concrete Composite Columns, 10th Pacific Conference on Earthquake Engineering, Nov. 6-8, Sydney, Australia.
Ricle, J., Paboojian, S.,and Bruin, W. 1992. ExperimentalStudy of Composite Columns Subjected to Seismic Loading Conditions. 10th World Conference on Earthquake Engineering,Balkema, Rotterdam.
Sezen, H. 2000, Seismic Behavior and Modeling of Reinforced Concrete Building Columns, PEER Report 2000/09, Pacific Earthquake Engineering Research Center, Berkeley, CA, USA.
Tall Building Initiative, 2011, Pacific Earthquake Engineering Research Center, University of California, Berkeley, CA, USA.